8 Radiation Sources

This chapter describes the parameters and performance of the radiation sources planned for NSLS-II. Continuing the tradition established by the existing NSLS, they span a very wide spectral range, from the far IR, down to 0.1 meV (equivalent to 1 cm^{-1}), to the very hard x-ray region, more than 300 keV. This is achieved by a combination of bending magnet sources, covering the IR, VUV, and soft x-ray range, and insertion device sources, covering the VUV through very hard x-ray range. They will achieve world leading levels of time average brightness and flux from the far IR through to ~20 keV, only being surpassed above ~20 to 25 keV by the performance of synchrotrons operating at higher energy (6 to 8 GeV).

As discussed in Chapter 6, the NSLS-II lattice contains 30 DBA cells, or 15 superperiods with alternating straight section lengths of 5 m and 8 m. The 5 m straights will have low beta functions and the 8 m straights somewhat higher beta functions. The resulting horizontal and vertical electron beam sizes and divergences in the center of the two types of straights, as well as in the center of the bend magnets, are given in Table 8.1.1. These beam sizes and divergences are already very small, and an option for even smaller beam sizes is discussed in Section 8.3.8. The beta functions also determine the allowed minimum vertical gap of an undulator and non-linear dynamic effects constrain the maximum length of the undulator, L. The minimum undulator gap and the undulator lengths for the devices described in this chapter were all chosen to satisfy these constraints.

All of the source properties described in this chapter assume a fully-damped horizontal emittance value of 0.55 nm-rad. This is the performance value for the NSLS-II storage ring when operating with a full complement of eight 7 m damping wigglers. The initial emittance value will be greater than this value, owing to operation with fewer damping wigglers, as discussed in Chapter 6.

Table 8.1.1 Electron Beam Size and Divergence at NSLS-II.

Type of source	5 m straight section	8 m straight section	Bend magnet
σ_x [μm]	38.5	99.5	44.2
$\sigma_{x'}$ [μrad]	14.2	5.48	63.1
σ_y [μm]	3.05	5.51	15.7
$\sigma_{y'}$ [μrad]	3.22	1.78	0.63

8.1 Insertion Devices

The goal in choosing the set of principal insertion device parameters is to provide a wide overall spectral coverage with insertion devices that target the photon energy ranges of interest for the experimental programs. It is expected that other parameter choices besides those outlined here may be specified to meet the needs of the science program as it evolves over time.

The set of insertion devices described includes hard x-ray, soft x-ray, and VUV undulators, x-ray damping wigglers, and high-energy superconducting wigglers. Their spectral brightness, flux, power, spatial and angular output properties, and polarization performance are described. These IDs produce high-brightness radiation spanning a large photon energy range, from the VUV (~10 eV) to the very hard x-ray (~300 keV). An R&D program focused on developing the required magnetic and mechanical design of these devices is presented in Chapter 12. Their effects on the properties of the NSLS-II storage ring and other accelerator physics issues are presented in Chapter 6.

The set of IDs discussed is not meant to be a complete set. Rather, these devices represent a possible set that might optimize the performance of the beamlines that are ultimately constructed. Once these beamlines are actually chosen, it is anticipated that, consistent with the philosophy of building beamlines dedicated to a given technique, the source will also be individually optimized for each application, as appropriate.

Other types of undulators and/or wigglers besides those discussed in this Chapter will also be considered during the preliminary engineering design phase of the project. These will include in-vacuum EPUs, to reach smaller magnetic gaps and thereby wider photon energy coverage, and quasi-periodicity, for both planar undulators and EPUs. In addition, revolver concepts, figure-8 type undulators, and long-period electromagnetic undulators will be considered. These concepts are discussed further in the description of the undulator R&D program in Chapter 12.

8.1.1 Planar Undulators

The hard x-ray undulators at NSLS-II will be planar designs and will produce linearly polarized radiation.

8.1.1.1 CPMU – U19

The baseline NSLS-II hard x-ray undulator is a Cryogenic Permanent Magnet Undulator with a period of 19 mm, referred to as U19. Cooling the CPMU's magnets to ~150 K increases its peak magnetic field strength by ~13%. Cooling a permanent magnet undulator to achieve higher performance is a quite recent development of the last few years, but has already undergone significant development. There are some remaining issues that require R&D to fully demonstrate a device with the capabilities described here, as discussed in Chapter 12. However, we are confident they can be addressed and so we specify a U19 device as the baseline hard x-ray undulator for NSLS-II.

8.1.1.1 SCU – U14

Superconducting undulator technology requires substantial R&D to demonstrate its viability and so SCUs are not specified as baseline devices for NSLS-II. We do plan to carry out an R&D program focused on pursuing SCUs using high temperature superconducting technology, as described in Chapter 12. If successful, it will enable x-ray undulators to be produced with both shorter periods and higher K than the U19 CPMU device. For example, a 14 mm period SCU, referred to as U14, has ~25% shorter period than U19 but will be able to achieve 10% higher K_{max}. Together, these increase the brightness by a factor of ~2 over that of U19, provide more continuous coverage as the field strength is tuned, and extend the performance to higher energies. The spectral properties of an SCU U14 device are described here in addition to those of the baseline CPMU U19 device in order to give an indication of the performance that would become possible with the successful development of this technology.

8.1.2 Elliptically Polarized Undulators

The NSLS-II soft x-ray and VUV insertion devices will be elliptically polarized undulators. These EPUs provide full ellipticity control of the radiated output from circular through linear, while only marginally reducing the brightness of the linearly polarized output, compared to pure planar undulators of the same period. In addition, these EPUs can also provide linearly polarized output with the polarization axis oriented either horizontally, vertically, or anywhere in between. As discussed in the soft x-ray beamline sections (see Chapter 11), these properties are extremely useful for separating various contributions to a given signal in an experiment.

8.1.2.1 Soft X-ray EPU – EPU45

The total length of the EPU45 undulator is specified as 4 m, corresponding to a single long device. However, this corresponds to only one of two proposed operating modes for these devices. In fact, for the soft x-ray beamlines discussed in Chapter 11, this 4 m total length would be comprised of two ~2 m EPUs and the appropriate steering magnets and diagnostics would be placed between the sections to allow a small (~0.25 m-rad) canting angle for the electron beam between them. As described in more detail in Chapter 11, this configuration will allow the two undulator sections to be set to two different polarizations, e.g., left circular and right circular, or horizontal linear and vertical linear. The angular separation provided by the canting will then permit fast switching between the chosen polarizations of the two EPUs, thereby enabling various types of polarization sensitive experiments to be performed with high sensitivity, as provided by lock-in detection methods for example. The accelerator issues associated with these, and other, canting angles are discussed briefly in Section 6.1 and will be addressed in more detail in the technical design phase of this project.

8.1.2.2 VUV EPU – EPU100

The harmonic content issue is particularly important in the case of the EPU100 owing to the intensity of the n >1 harmonics, which are comparable to or even greater than the n = 1 fundamental, as shown below. As a result, the EPU100, which produces vacuum ultraviolet radiation, will almost certainly need to be quasi-periodic, an issue that will be addressed during the R&D and technical design phases, as discussed in Chapter 12.

8.1.3 Wigglers

Classes of experiments that require continuous x-ray spectra, sizable x-ray beams, or very hard x-rays, such as EXAFS, powder diffraction, x-ray topography, x-ray photoemission, x-ray standing waves, high pressure, and x-ray footprinting, to name some, will benefit from the availability of x-ray beamlines that view damping wiggler sources. Superconducting wigglers will be the preferred source for those experiments requiring very hard x-rays, up to ~300 keV. All wiggler sources at NSLS-II are expected to be in high demand.

8.1.3.1 Damping Wiggler – DW100

The damping wigglers will produce the highest flux of any NSLS-II source out to ~30 keV and will also have excellent brightness. They are expected to be the premier source for experiments above ~5 keV that do not require the ultra-high brightness and small beams produced by the hard x-ray undulators.

8.1.3.2 Superconducting Wiggler – SCW60

The highest energy photons will be produced by very high field, short period, wigglers. The radiation will be broadband with high power at high x-ray energies, covering the 20 to 300 keV energy range. The selected device has a wiggler field of 6.0 T and a period length of only 60 mm so that the flux and brightness are as high as possible. The combination of high field and small period requires a superconducting wiggler design that pushes the limit of presently achievable current density, an issue that will be addressed during the technical design phase. Specifications of other similar high SCWs that are currently in service at medium energy synchrotrons are listed in Table 8.1.2.

Table 8.1.2 Some Working SCWs Similar in Specifications to Proposed and Alternative NSLS-II Wigglers.

Facility	Manufacturer	Field(T)	Period (cm)	# full-field poles
NSLS X17	Oxford	6	17.4	5
BESSY II	Novosibirsk	7	14.8	13
CLS	Novosibirsk	4.2	4.8	25
ELETTRA	Novosibirsk	3.6	6.4	45
MAX lab	Custom	3.5	6.1	47

The SCW60 will outperform other options at energies above 30 keV. The deflection parameter, K, is chosen to be wide enough to generate a large horizontal beam profile of a more than 0.5 m at 50 m from the source point. This allows splitting of the fan into multiple experimental hutches, as discussed in Chapter 11.

8.2 Bend Magnets

The NSLS-II bending magnets will have a relatively low critical energy (2.4 keV), and will be excellent sources for low photon energies, below 10 keV. It is expected that the available bend magnet ports will be allocated primarily to VUV and soft x-ray uses, as well as infrared uses. Those classes of experiments that require access to harder x-rays (energy >~5 keV) are better suited to damping wiggler sources.

The NSLS-II bend magnets will provide very stable beams. The relatively low emitted power simplifies the cooling requirements on the optics, although it does not eliminate the need to provide cooling. The brightness provided by the NSLS-II dipole sources will be three orders of magnitude higher than that of the present NSLS dipoles (extending up to ~12 keV) and their flux will also show some improvement (extending up to ~4 keV), as shown in Table 8.2.1. Indeed, the NSLS-II bend magnets will provide almost twice the flux of the ALS conventional bend magnets (i.e., not the superbends) and offer even larger improvements in source brightness. Thus, aspects of the very successful ALS research programs based on bend magnet illumination can be developed at NSLS-II, although the distribution of beamlines and end stations will be determined by the strengths and interests of the NSLS-II user community.

Table 8.2.1 Comparison of Bend Magnet Sources.

	NSLS-II Bend Magnet		ALS Conventional Bend Magnet		NSLS X-Ray Bend Magnet		NSLS VUV Bend Magnet	
Energy	Flux	Brightness	Flux	Brightness	Flux	Brightness	Flux	Brightness
1000 eV	3.3×10^{13}	1.5×10^{16}	2.1×10^{13}	1.5×10^{15}	1.4×10^{13}	1.3×10^{14}	6.0×10^{12}	1.1×10^{13}
100 eV	2.5×10^{13}	8.0×10^{15}	1.5×10^{13}	7.5×10^{14}	8.0×10^{12}	7.0×10^{13}	1.3×10^{13}	9.0×10^{13}
10 eV	1.3×10^{13}	3.7×10^{15}	7.2×10^{12}	3.4×10^{14}	3.8×10^{12}	2.8×10^{13}	7.7×10^{12}	4.4×10^{12}
1 eV	5.9×10^{12}	1.7×10^{15}	3.4×10^{12}	1.6×10^{14}	1.8×10^{12}	1.3×10^{13}	3.7×10^{12}	2.0×10^{12}
0.1 eV	2.8×10^{12}	8.0×10^{14}	1.6×10^{12}	7.3×10^{13}	8.4×10^{11}	6.1×10^{12}	1.8×10^{12}	9.4×10^{11}

ALS parameters assume top-off mode operation at 500 mA stored current. Flux is in units of ph/s/0.1%BW and brightness is in units of ph/s/0.1%BW/mm^2/mrad^2.

The special considerations required for collecting infrared radiation produced by the bend magnets is discussed in detail in Section 8.4.

8.3 Parameters and Performance of Radiation Sources

The basic parameters characterizing the IDs and bending magnet sources are listed in Table 8.3.1. In the case of the NSLS-II bend magnet, the total power value is actually the power per horizontal mrad.

Table 8.3.1 Basic Parameters of NSLS-II Radiation Sources for Storage Ring Operation at 3.0 GeV and 500 mA.

	U14	U19	EPU45	EPU100	DW100	SCW60	Bend Magnet
Type	SCU	CPMU	EPU	EPU	PMW	SCW	Bend
Photon energy range [keV]	Hard x-ray (1.8–30)	Hard x-ray (1.5–20)	Soft x-ray (0.180 – 7)	VUV (0.008 – 4)	Broadband (<0.010 - 100)	Very hard x-ray (<0.010 – 200)	Soft and low-energy x-ray (<0.010 – 12)
Type of straight section	5 m	5 m	5 m	5 m	8 m	5 m	
Period length, λ_U [mm]	14	19	45	100	100	60	
Total device length [m]	2.0	3.0	4.0	4.0	7.0	1.0	
Number of periods	143	158	89	40	70	17	
Minimum magnetic gap [mm]	5	5	10	10	15	TBD	
Peak magnetic field strength in linear mode, B [T]	1.68	1.14	1.03	1.50	1.80	6.0	0.40
Max K_y*, linear mode	2.20	2.03	4.33	14.01	16.81	33.62	
Peak magnetic field strength in circular mode, B [T]			0.64	1.15			
Max K_y*, circular mode			2.69	10.74			
Minimum $h\nu$ fundamental [keV]	1.79	1.47	0.183	0.0086			
$h\nu$ critical [keV]					10.77	35.91	2.39
Maximum total power [kW]	16.08	11.18	12.09	25.64	64.60	102.55	0.0228
On-axis power density [kW/mrad^2]	103.70	77.86	40.03	26.33	55.30	43.9	0.0879
Horizontal angular power density [kW/mrad]							0.023

*K = 0.934 B[T] λ_u[cm]

8.3.1 Brightness

For many experiments, especially those involving imaging or microscopy, where, for example, the beam must be focused down to a small spot, the key figure of merit of user radiation sources is their time average brightness. This is the flux output per unit bandwidth, per unit source area, and per unit solid angular divergence. Undulators and wigglers are excellent sources of high brightness radiation. The brightness of the base set of radiation sources for NSLS-II is is shown in Figure 8.3.1. For the undulators, the tuning curves of harmonics 1, 3, 5, 7, and 9 are shown. These tuning curves show the variation of the peak brightness of the undulator harmonics as the magnetic field strength, and hence K parameter, is varied from K_{max}, listed for each undulator in Table 8.3.1, down to K_{min} ~0.4.

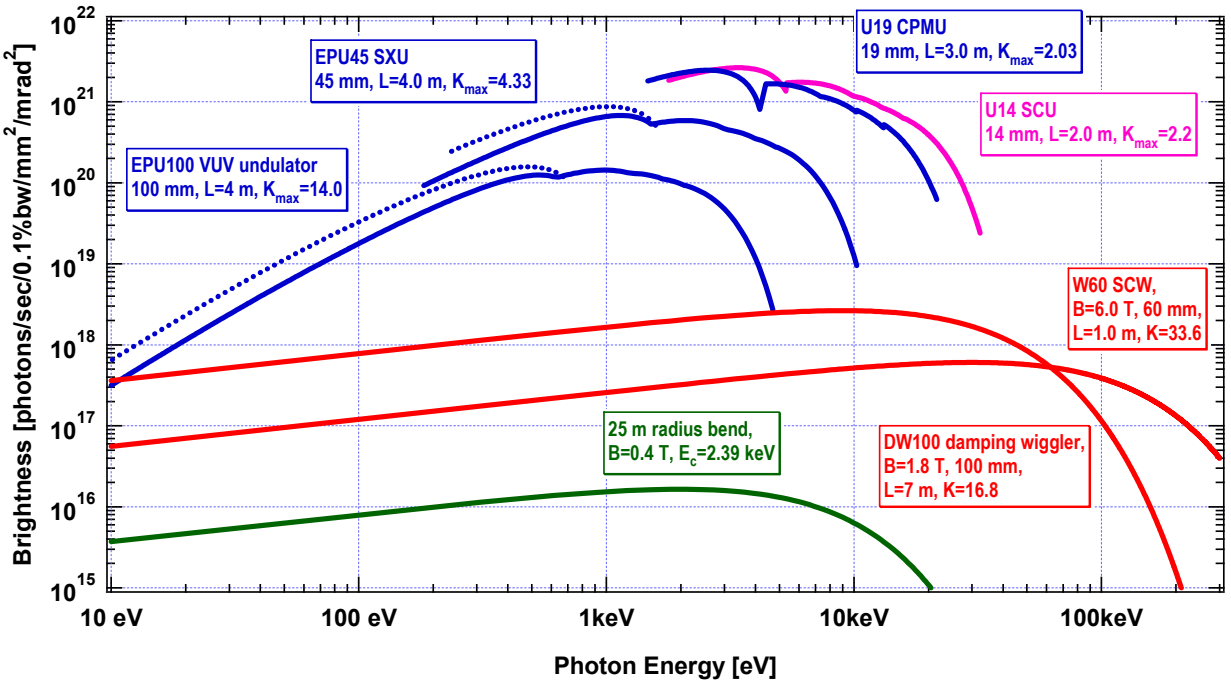

Figure 8.3.1 Brightness vs. photon energy for various devices at NSLS-II. Ring parameters: 3.0 GeV, 0.5 A, ε_h=0.55 nm, ε_v=0.01 nm, energy spread=0.001; Straight section parameters: 5 m length: ε_h=2.7 m, β_v=0.945 m; 8 m length: β_h=18.2 m, β_v=3.09 m; α_h=α_v=η_h=η_v=η'_h=η'_v=0; Bend magnet parameters: β_h=0.65 m, β_v=25.1 m, α_h=0.032, α_v=-0.044, η_h=0.04 m, η'_h=0.056, η_v=η'_v=0.

The brightness of the U14 and U19 hard x-ray undulators is the highest of any devices proposed for NSLS-II. This is due in part to the short period length of these devices, thereby increasing the number of periods contributing to the flux output, and in part to the short output wavelengths compared to the soft x-ray (EPU45) and VUV (EPU100) undulators. For diffraction-limited undulator radiation, which characterizes a good portion of the range of these four undulators, the brightness varies inversely as the square of the output wavelength. Note that the brightness of the hard x-ray undulators (U14 and U19) exceeds the 10^{21} ph/s/0.1%BW/mm^2/mrad^2 level.

The wigglers provide broadband, high brightness sources of x-ray radiation. Each of the wigglers shown in Figure 8.3.1 covers nearly the entire photon energy range shown. The superconducting wiggler SCW60 is optimized for very high-energy x-ray work (i.e., above ~60 keV), while the damping wiggler DW100 is a high-flux, hard x-ray source with smooth spectral output extending down through the soft x-ray and VUV photon energy ranges. Note that the EPU100 undulator and DW100 wiggler devices have the same period length (100 mm) and comparable magnetic field strength (1.5 T for EPU100 vs. 1.8 T for DW100). The difference in their brightness and flux curves, other than their difference in length (4 m for EPU100 vs. 7 m for DW100) arises in the difference between the standard undulator and wiggler flux and brightness formulae: the undulator values represent the peaks (in photon energy) of a widely-varying intensity spectrum, while the wiggler values represent an average value. For use of the low-n harmonics (n = 1, 3, 5, 7, or 9), the undulator formula is most useful, while for the high-n harmonics (n >20 or so), the wiggler formula is more appropriate.

Figure 8.3.1 shows the source brightness of the EPU45 and EPU100, in two polarization modes: helical (or circular), shown as dotted lines, and linear, shown as solid lines. The circular polarized mode has intensity only in the fundamental and is slightly brighter than the linearly polarized mode at the same energy. It is expected that this mode will be used for all work below 2 keV for the EPU45 and below 850 eV for the EPU100, unless linearly polarized light is specifically required.

The NSLS-II bending magnet spectral brightness curve is also shown in Figure 8.3.1. The bending magnet spectrum is a bright source which extends from the infrared to the hard x-ray. These sources will be useful up to a few times the critical energy of 2.39 keV, i.e., up to ~10 keV. The bending magnet brightness peaks at ~2 keV, making it an ideal broadband source in the soft x-ray (0.1–2 keV) and low-energy x-ray (2–5 keV) ranges.

8.3.2 Flux

For those experiments which do not require a very collimated and/or focused beam, the photon spectral flux is the key figure of merit. This is the number of photons per unit bandwidth per unit time. Figure 8.3.2 shows the flux for the NSLS-II radiation sources. The maximum flux is ~1.5×10^{16} ph/s/0.1%BW, reached by the damping wiggler DW100 at ~3 keV. The hard x-ray undulators U14 and U19 reach a flux of ~5×10^{15} ph/s/0.1%BW at an energy of ~2 keV. As discussed in Section 8.2, the bend magnets at NSLS-II will be superlative sources of high brightness and high flux radiation in the VUV and soft x-ray energy range. For both wigglers and bend magnets, a horizontal collection of 3 mrad is typical (Figure 8.3.2), although larger horizontal angular fans—e.g., up to 10 mrad—could be made available, if required.

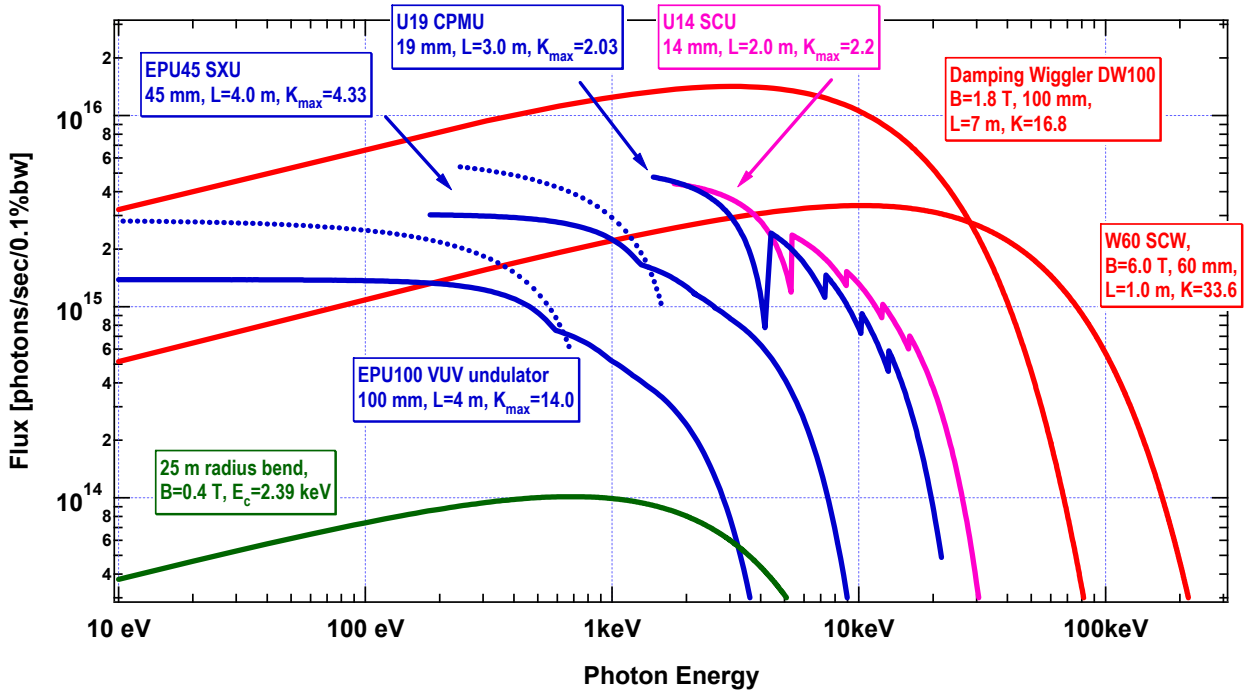

Figure 8.3.2 Flux output of various devices at NSLS-II vs. photon energy. See the caption to Figure 8.3.1 for a listing of accelerator parameters used to calculate the flux curves shown here."

8.3.3 Power

Table 8.3.1 gives the maximum total output power of the NSLS-II radiation sources and Figure 8.3.3 shows how the total output power output of the undulators varies as their K value is changes from K_{min} (taken to be ~0.4) to K_{max}, as given in Table 8.3.1. For reference, the corresponding energy of the photons' radiation in the fundamental as a function of K is also given. The photon energy of harmonic n is n times that of the fundamental.

The total power radiated by the undulators at their maximum K settings (i.e., at minimum magnetic gap) is in the 10–30 kW range. The total power output from the NSLS-II wigglers is higher than that of the

undulators, at nearly 65 kW, while that of the NSLS-II bend magnet is very much less, at only ~23 W per horizontal mrad (see Table 8.3.1). Figure 8.3.3 also shows that the total output power increases by about a factor of 2 when operating in circular mode compared to linear mode for the EPUs. The engineering challenges of handling the high heat loads in the insertion device front ends are detailed in Section 7.4.

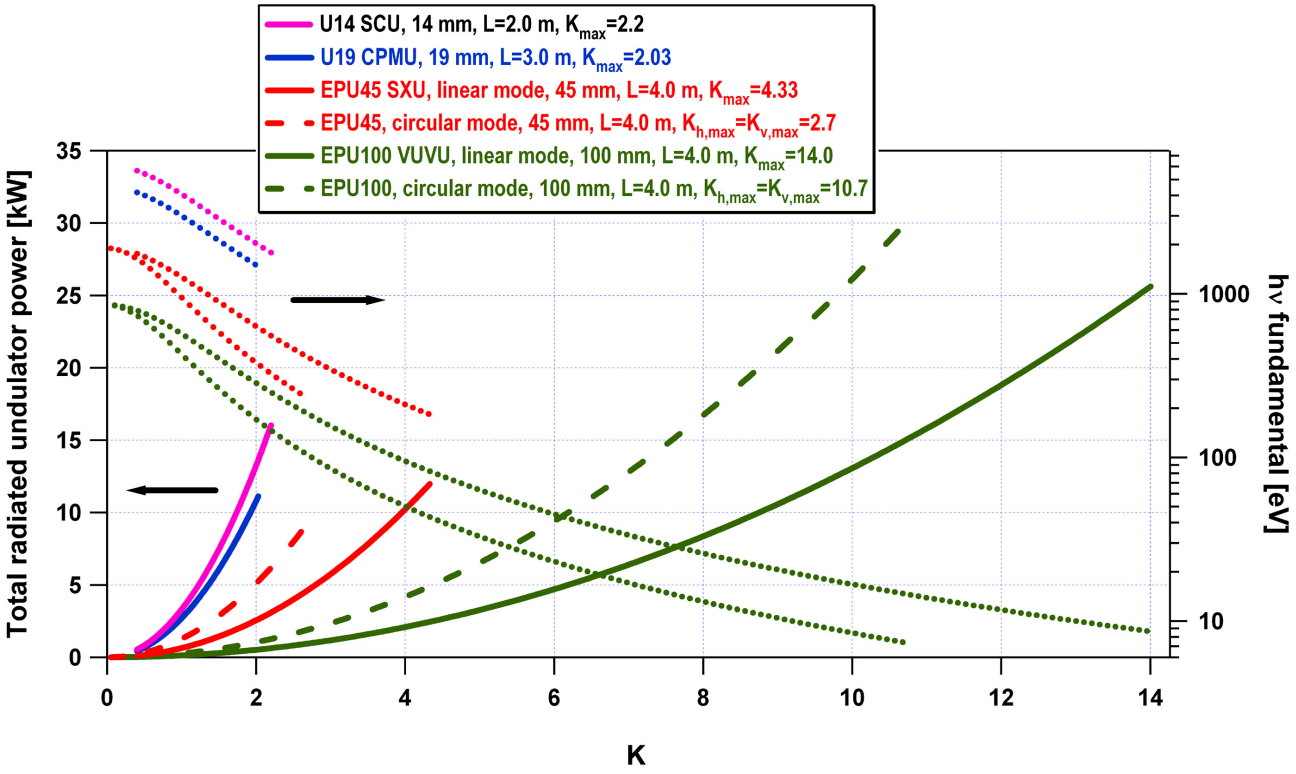

Figure 8.3.3 Total output power of the NSLS-II undulators as a function of the undulator parameter, K.

8.3.4 Power Density

Table 8.3.1 gives the maximum (on-axis) angular power density of the NSLS-II radiation sources; Figure 8.3.4 shows how the maximum angular power density of the undulators varies as their K value changes from K_{min} (taken to be ~0.4) to K_{max}, as given in Table 8.3.1. For reference, the corresponding energy of the photons radiated in the fundamental as a function of K is also given. The energy of harmonic n is n times that of the fundamental. The maximum undulator angular power density radiated by the undulators at their maximum K settings (i.e., at minimum magnetic gap) varies from 25 to 100 kW/mrad^2. The wiggler angular power density output is in the 25–55 kW/mrad^2 range, while the bend magnet value is again very much less, at 88 W/mrad^2.

Figure 8.3.4 also shows that the output angular power density of the EPUs in circular polarization mode is much lower than in linear polarization mode, and has a different dependence on K. This is primarily because in circular mode there are no higher harmonics, just the fundamental. An advantage of the circular polarization mode is the lower output power density, which simplifies the design and operation of high energy-resolution beamlines by reducing the thermal deformations of the optical elements (see Chapter 11).

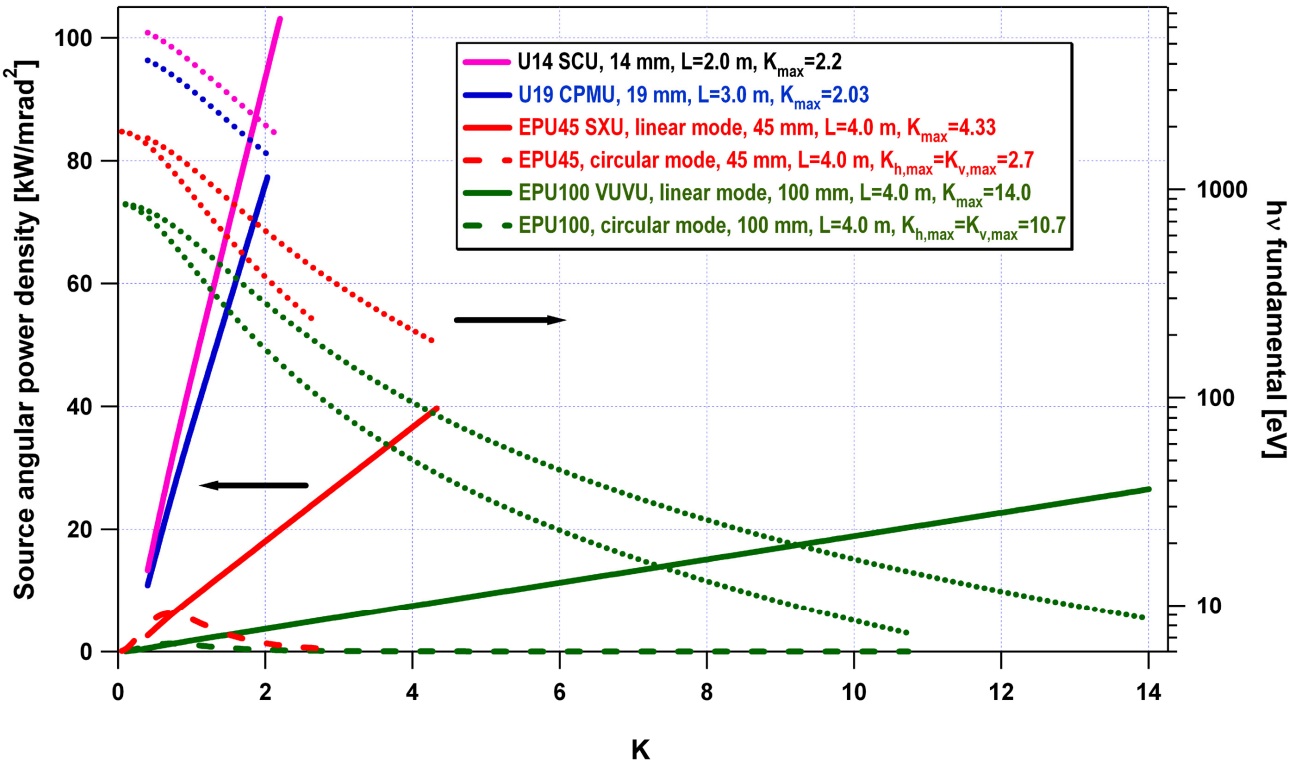

Figure 8.3.4 Angular power density versus undulator parameter, K, for the NSLS-II undulators.

8.3.5 Photon Beam Size

The 1-σ effective photon beam size of the NSLS-II undulators is shown in Figure 8.3.5 as a function of photon energy. The lowest, straight (on a log-log graph) gray lines show the "natural" photon beam size, which is the size of a diffraction-limited photon beam for a zero emittance (and therefore zero size) electron beam. This diffraction-limited, "natural" photon beam size σ_{photon} is given by

$$\sigma_{photon} = \frac{1}{4\pi}\sqrt{2L\lambda} \quad . \tag{8.1-2}$$

One measure of the effective photon beam size, σ_{eff}, is given by the quadrature sum of the electron ($\sigma_{electron}$) and photon, σ_{photon}, contributions:

$$\sigma_{eff} = \sqrt{\sigma_{electron}^{\ 2} + \sigma_{photon}^{\ 2}} \quad . \tag{8.1-3}$$

The green, red, and blue curves show σ_{eff} for the NSLS-II undulators in the vertical and horizontal planes, as labeled. Clearly, the undulator radiation is nearly diffraction-limited in the vertical plane over a wide photon energy range from 10 eV to ~2 keV. The deviation of the effective source size from the natural, diffraction-limited value is due to the contribution of the small, but finite, electron beam size. The effective beam size in the horizontal plane is approximately an order of magnitude greater than the natural, diffraction-limited value at 10 keV, but at 10 eV is nearly diffraction-limited.

It should be noted that the beam sizes shown in Figure 8.3.5 were calculated for the current baseline electron beam sizes given in Table 8.1.1. If it proves possible to use the smaller horizontal beta function in the

5 m straights, discussed in Section 8.3.8, there would be a corresponding reduction the horizontal photon beam sizes shown in Figure 8.3.5, and a corresponding increase in the degree of coherence.

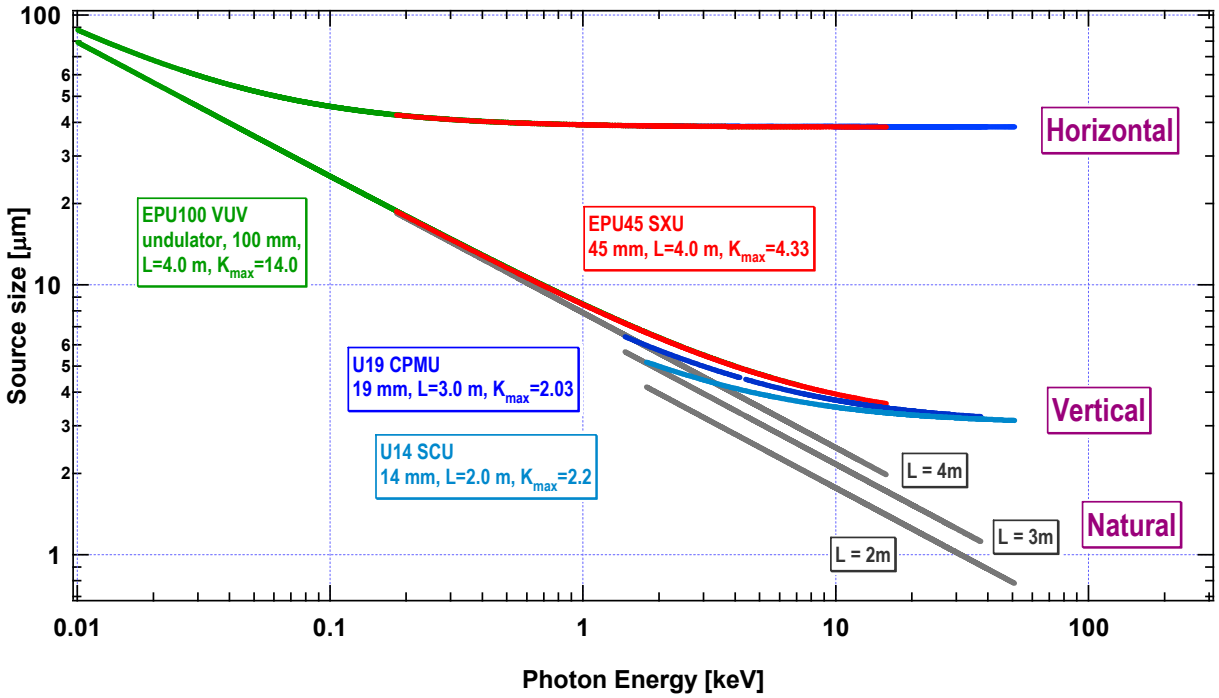

Figure 8.3.5 Photon beam source size in the horizontal and vertical directions for the various NSLS-II devices. The straight (gray) lines represent the diffraction-limited values for the various devices (i.e., the zero electron beam emittance limit).

8.3.6 Photon Beam Angular Divergence

The 1-σ effective photon beam angular divergence of the NSLS-II undulators is shown in Figure 8.3.6 as a function of photon energy. The lowest, straight (on a log-log graph) gray lines show the "natural" photon beam angular divergence, which is the angular divergence of a diffraction-limited photon beam for a zero-emittance (and therefore zero angular divergence) electron beam. The diffraction-limited, "natural" photon beam angular divergence σ'_{photon} is given by

$$\sigma'_{photon} = \sqrt{\frac{\lambda}{2L}} \tag{8.1-4}$$

and the effective photon beam angular divergence σ'_{eff} is again given by the quadrature sum of the electron ($\sigma'_{electron}$) and photon (σ'_{photon}) contributions:

$$\sigma'_{eff} = \sqrt{\sigma'^{\,2}_{electron} + \sigma'^{\,2}_{photon}} \quad . \tag{8.1-5}$$

The green, red, and blue curves in Figure 8.3.6 show σ'_{eff} for the NSLS-II undulators in the vertical and horizontal planes, as labeled. As in Figure 8.3.5 for beam size, Figure 8.3.6 shows that the angular divergence of the undulator radiation from NSLS-II undulators is nearly diffraction-limited in the vertical plane, and only somewhat less so in the horizontal plane, over the wide photon energy range from 10 eV to ~2 keV. The deviation of the effective source angular divergence from the natural, diffraction-limited, value is due in part to the contribution of the tiny, but finite, beam angular divergence of the NSLS-II electron beam. In the

horizontal plane, the effective beam angular divergence is approximately a factor of 2 or 3 greater than the natural, diffraction-limited, value at 10 keV, but is nearly diffraction-limited at 10eV.

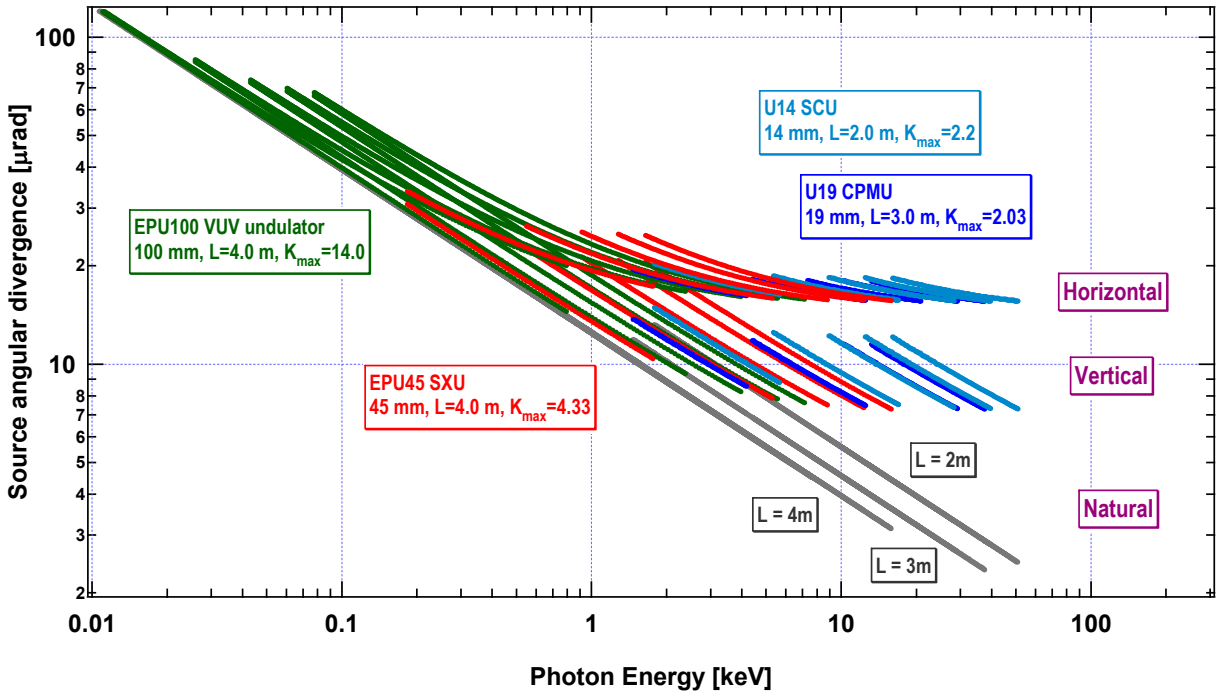

Figure 8.3.6 The angular divergence of the photon beam at NSLS-II devices.

The angular divergence is also limited by the finite energy spread of the electron beam. A noteworthy feature of Figure 8.3.6 is that the angular divergence of the various harmonics for a given undulator is approximately equal to that of the fundamental of that undulator. That is, it appears, empirically, that the angular divergence of undulator harmonic n is given by

$$\sigma'_n \approx \sqrt{\frac{\lambda_1}{2L}} \tag{8.1-6}$$

for n = 1, 3, 5, 7, or 9, in both the horizontal and vertical planes. This value is $\sqrt{\lambda_1}/\lambda_n = \sqrt{n}$ times larger than the natural, diffraction-limited angular divergence.

Thus, the limiting factor governing the vertical angular spread of the U14 and U19 undulators is the finite energy spread of the electron beam, which for the fully-damped case is $\delta E/E \sim 0.001$. Figure 8.3.7 illustrates this effect for the U14 SCU for three values of energy spread: 0, 0.0005, and 0.001. The difference between the natural, diffraction-limited, vertical angular divergence and the curve labeled $\delta E/E = 0$ is the contribution from the finite vertical angular spread of the electron beam. The difference between the $\delta E/E = 0$, $\delta E/E = 0.0005$, and $\delta E/E = 0.001$ curves is the contribution from the specified electron energy spread. Figure 8.3.7 clearly demonstrates that the vertical angular divergence of the U14 fundamental is determined by the combined contributions of the natural and electron beam divergences, but that the vertical angular divergence of the higher harmonics (n = 3, 5, 7, and 9) is mostly determined by the effect of electron energy spread. Note however, as can be seen in Figure 8.3.6, that whereas the effect of energy spread is significant for the U14 and U19 undulators, it has a much smaller effect on the angular divergence of the soft x-ray and VUV undulators.

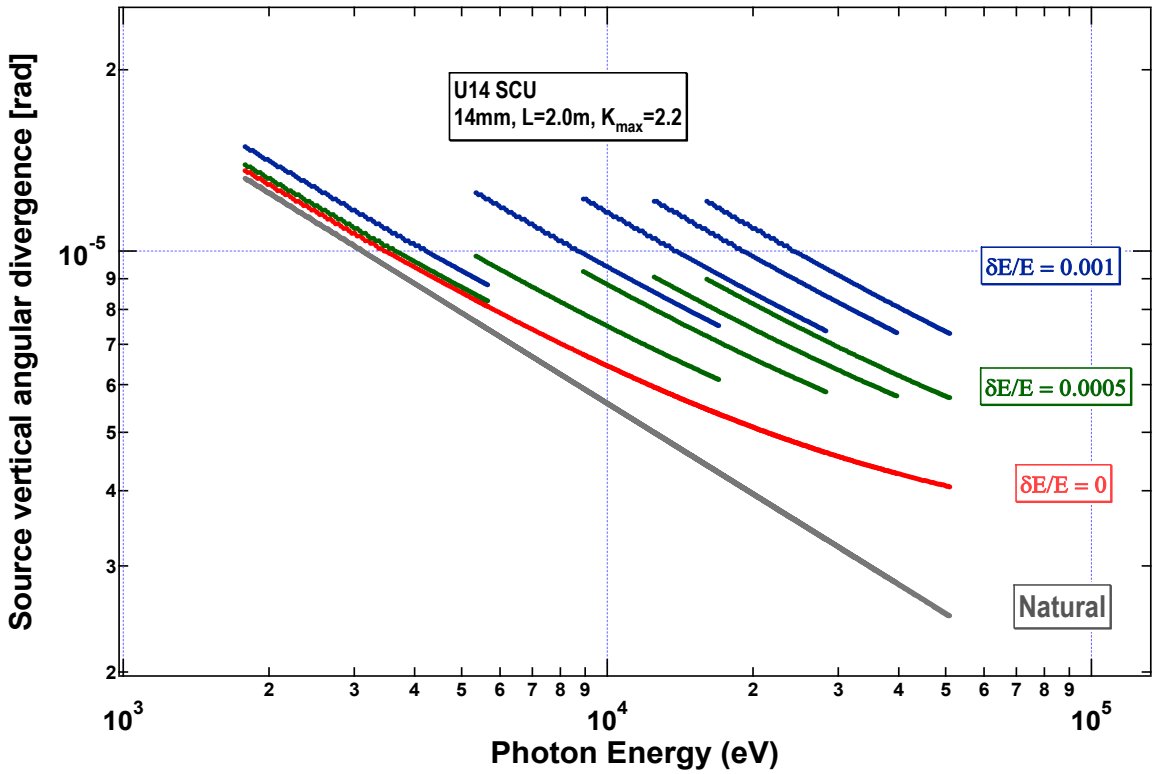

Figure 8.3.7 The vertical angular divergence for the 14 mm SCU device vs. photon energy for different values of the energy spread of the electron beam. The straight (gray) line is the diffraction limit, and the deviation from this line at higher energies for zero energy spread is a result of the finite electron beam divergence.

8.3.7 Effect of Increasing Undulator Length

One way to increase undulator source brightness and flux is to increase the overall length, i.e., to increase the number of undulator periods. Of course, accelerator physical constraints must be obeyed, including the minimum magnetic gap vs. length, the overall maximum ID straight section length, and limits set by collective effects. For a low emittance electron beam, the length dependence of the brightness should be similar to that of the flux, since for a diffraction-limited photon beam the denominator in the brightness expression depends only on the emitted wavelength. It turns out that the linear dependence of brightness vs. undulator length applies only to the case of zero electron energy spread, as demonstrated for the 5th harmonic of the U19 CPMU by the uppermost solid curve in Figure 8.3.8. For non-zero energy spread values, this dependence becomes sublinear. For example, for 0.001% electron beam energy spread, a 2 m long U19 CPMU is 2.1 times brighter than a 1 m long device, but a 6 m long device is only 1.75 times brighter than a 3 m long device. Moreover, the brightness penalty for finite energy spread is rather severe: for 0.001% energy spread, the brightness reduction compared to zero energy spread ranges from a 35% reduction for a 1 m long U19 CPMU to more than 70% reduction for a 7 m long device. For 0.002% energy spread, the corresponding reduction fractions are 60% and 85%.

It is clear that the origin of the energy-spread-related brightness reduction lies mostly in the vertical divergence angle, as pointed out Section 8.3.6 above. This effect is greater for higher harmonics than lower ones. Shown by dotted lines in Figure 8.3.8 are the brightness vs. undulator length curves for the 3rd harmonic at 3.6 GeV electron energy. The zero-energy-spread curves are nearly identical, but the 0.001% and 0.002% energy spread curves are more than 1.5 times brighter than the 5th harmonic curves at 3.0 GeV (solid lines).

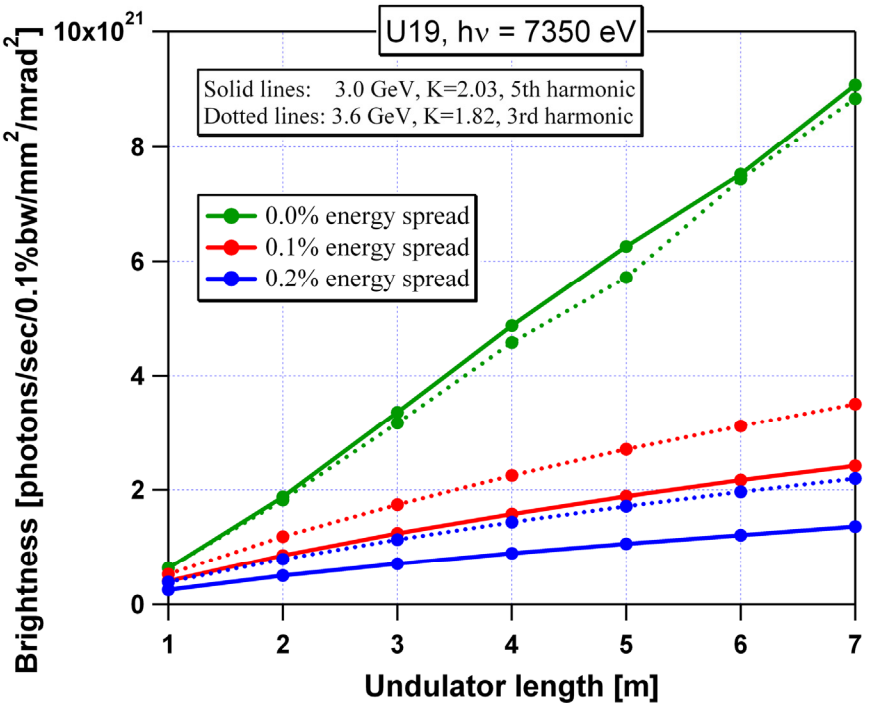

Figure 8.3.8 On-axis brightness of the U19 undulator at 7350 eV photon energy as a function of undulator length, for the 5th harmonic at 3 GeV (K = 2.03, solid lines) and the 3rd harmonic at 3.6 GeV (K = 1.82, dotted lines).

8.3.8 Effect of Possible Reduction of Horizontal β-Function

We are investigating whether the horizontal β-function at the center of the 5m ID straight sections might be able to be reduced by about a factor of 10 from baseline value, i.e., from 2.7 m to ~0.3 m. Although this would only increase the brightness by ~20% for the U19 CPMU and U14 SCU undulators, it would have a significant effect in reducing the horizontal source size from the already unprecedented low value of 38.5 μm (see Table 8.1.1) to an even lower value of 12.2 μm. This would lead to nearly round photon beams, given the vertical size of 3.05 μm. Such tiny and nearly round beams are a decided advantage for microscopy applications, such as the nanoprobe beamline described in Chapter 11.

8.3.9 Options for Multiple U14 or U19 Undulators in a Single ID Straight Section

It may also be feasible to insert multiple U14 or U19 undulators in a single 5 m or 8 m ID straight section by including additional focusing magnets to focus the electron beam in the centers of these multiple undulators and so maintain small beta functions throughout their length. One scenario would enable two 2 m long U14 SCUs to be installed in a 5 m long ID straight section with β_h = 0.3 m and β_v = 0.945 m, as described for a single undulator above. Another scenario would enable either three 2 m long U14 SCUs or two 3 m long U19 CPMUs to be installed in an 8 m long ID straight section, with β_h = 3m and β_v = 3m. The brightness increase for either of these scenarios involving the U19 CPMU at the low energy end of its tuning curve is ~60%, whereas that for scenarios involving the U14 SCU is ~150%. A bigger advantage is the increase in flux, which is linear in undulator length, and thus would increase a factor of 2 for two U19 devices in an 8 m straight and a factor of 3 for three U14 devices in an 8 m straight. This would be especially advantageous for flux-starved experiments, such as those attempting to perform spectroscopy with 0.1 meV energy resolution, as outlined in Chapter 11.

8.3.10 Optimization of Insertion Devices for Specific Beamlines

To maximize overall beamline performance of NSLS-II undulator beamlines, the parameters of the undulator should be matched to those of the beamline, and both should match the experiments that they serve. The specificity of experiments at the various beamlines ranges widely, as does the specificity of the various beamlines. Therefore, the parameters of the undulators shown in this Chapter are intended to be representative choices to serve broad photon energy ranges, and not necessarily the exact values that would be chosen for a specific beamline.

As an example of the optimization process needed to match undulator and beamline parameters, we consider the needs of the Inelastic X-Ray Scattering Beamline. The ultra high resolution IXS experiments would primarily utilize a photon energy of 9 keV and so the undulator parameters should optimize the source brightness at this energy. Figure 8.3.9 shows the brightness of the various harmonics of candidate CPMUs in a photon energy region centered at 9 keV. The CPMUs considered are of fixed overall length (3 m), but with periods of 16, 17.5, 19, and 21 mm, a range which brackets the canonical CPMU period length of 19 mm for U19.

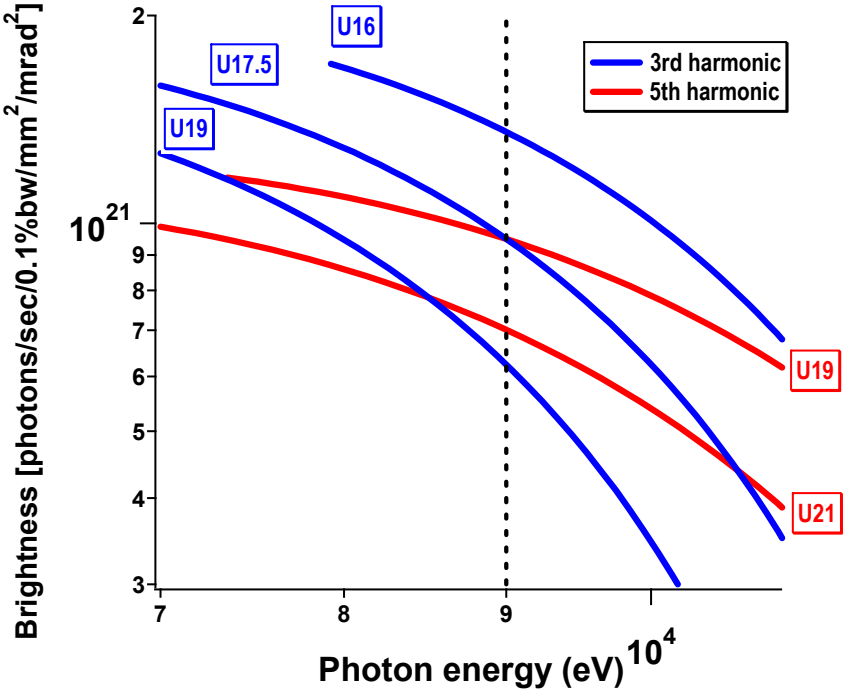

Figure 8.3.9 Possible candidate devices that optimize the brightness of undulators around 9 keV.

Figure 8.3.9 shows the brightness of third and fifth harmonic emission from these candidate CPMUs. Fundamental (first harmonic) emission does not reach 9 keV for any of the CPMU period lengths considered, and the seventh and higher harmonics produce lower brightness at 9 keV than the third and fifth. The optimum undulator parameter choice to maximize source brightness at 9keV is the third harmonic of the 16 mm period CPMU (uppermost blue curve in Figure 8.3.9). Note that it may be possible to further optimize this brightness by going to a slightly shorter period (e.g., 14.5 mm) before the minimum photon energy for the third harmonic exceeds 9 keV. Of course, an additional gain in brightness would also be realized from the third harmonic of the 2 m, 14 mm period superconducting undulator if such a device were to be developed.

The figure of merit for the source for certain experiments, and their beamlines, might be flux rather than brightness. For such experiments, a similar optimization process should occur. The source flux of the various harmonics of candidate CPMUs in a photon energy region centered at 9 keV is shown in Figure 8.3.10. As is

typical of undulator sources, the differences in flux are smaller than the differences in brightness. In this case (and in general), the optimum combination of undulator period length and harmonic is the same for flux optimization and brightness optimization: third harmonic of the 16 mm period CPMU. In the case of flux, the fifth harmonic of the 19 mm period undulator is only slightly inferior to the optimum combination.

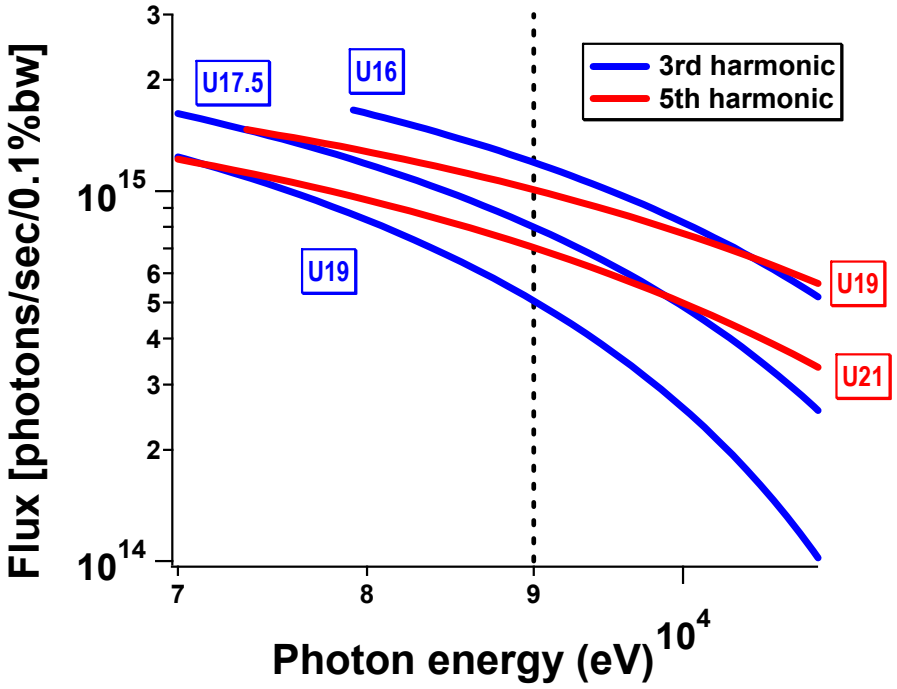

Figure 8.3.10 The source flux of the various harmonics of candidate CPMUs in a photon energy region centered at 9 keV.

.

8.4 Infrared

The intrinsic infrared brightness of most synchrotron storage ring sources is determined entirely by the circulating beam current. This is certainly the case for the low emittance electron beam of the NSLS-II storage ring, and the goal of 500 mA beam current is very attractive from the standpoint of infrared performance. The ring is designed for an extremely stable beam; an important characteristic for the standard rapid-scan interferometric techniques employed in most infrared spectroscopies. But designing an optical extraction configuration that preserves the brightness, while meeting mechanical and accelerator design constraints, can be quite difficult. Typically, the large angular collection needed to achieve an acceptable performance involves nonstandard construction geometries for the dipole chambers. These, in turn, can affect the beam impedance and lead to instabilities. A careful impedance analysis will be integral to the design of any dipole chamber intended for extracting infrared radiation, and efforts are underway to treat this issue quantitatively.

It is well known that dipole (bending) magnets produce infrared radiation by two distinct mechanisms: the conventional synchrotron radiation (bending magnet radiation) is produced in the body of the magnet, whereas edge radiation is produced as electrons enter or exit a dipole's magnetic field [8.4.1]. Infrared beamlines have been built to utilize one or the other of these source types, and sometimes both. For reasons outlined later in this section, we plan to meet most of the source requirements using bending magnet radiation, but also plan to collect and extract edge radiation. The beamline design and performance analysis described in Chapter 11 will take both source types into account.

8.4.1 Bending Magnet Source

The collection efficiency for conventional dipole bend radiation is determined by the natural opening angle for synchrotron radiation in the long wavelength limit. For a wavelength λ and bend radius ρ, the RMS half-angle is defined as:

$$\theta_\lambda = \left(\frac{3}{4\pi} \frac{\lambda}{\rho} \right)^{1/3} . \qquad (8.4\text{-}1)$$

From this expression we see that the large bending radius (ρ ~25 m) of NSLS-II dipoles causes the infrared to be emitted into angles 2.35 times smaller than for the existing NSLS VUV/IR ring (ρ ~1.9 m). Thus, the performance for NSLS-II with 38 mrad extraction would be identical to a 90 mrad extraction from the VUV/IR ring. A study of the NSLS-II dipole design indicates that a horizontal extraction of 50 mrad is achievable (plus an additional 5 mrad on the "negative side", useful for collecting edge radiation). This is based on an infrared extraction where the second dipole in a DBA cell is used in order to stay clear of any potential insertion device beamline (Figure 8.4.1). The large bending radius makes extraction increasingly difficult as one continues toward the second half of a dipole, giving rise to the 50 mrad horizontal collection limit.

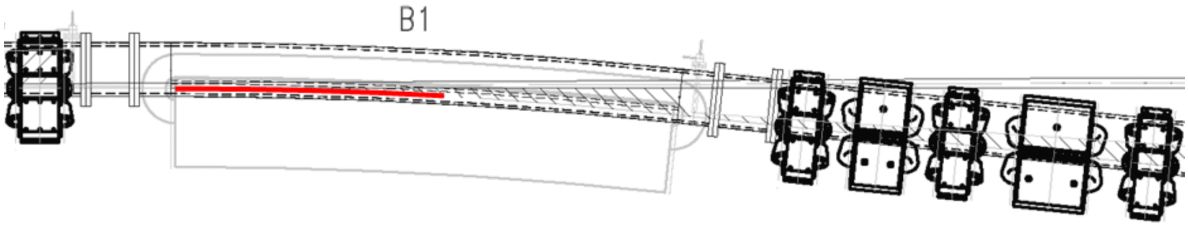

Figure 8.4.1 Drawing of the second dipole magnet in the NSLS-II DBA 30 lattice. Red line indicates the candidate IR source orbit segment. Approximately 50 mrad of horizontal collection appears feasible, including the zero degree segment for edge radiation.

The standard NSLS-II dipole bending magnets allow a vertical chamber dimension of ~25 mm and represent another constraint for infrared, limiting the vertical collection to approximately 16 mrad (the value varies from 12 mrad up to 20 mrad due to the large source depth). While this is adequate for mid-infrared spectroscopy as used in chemical imaging, it limits the performance for far-infrared spectroscopy due to the relatively large angles into which this radiation is emitted. Therefore, we are planning for a second dipole magnet design for use on far-infrared ports. This dipole would have a ~60 mm (or larger) gap and would accept a dipole chamber providing an average 32 mrad of vertical collection (and potentially up to 48 mrad with a larger dipole gap). The need for such a large aperture port becomes even more apparent when one considers the shielding effects of a conducting dipole vacuum chamber. The subject has been treated most thoroughly by Bosch [8.4.2] who confirmed (theoretically) that bending magnet radiation is suppressed for wavelengths greater than an effective cutoff value given by $\lambda_c=(h^3/\rho)^{1/2}$ where h is the chamber height and ρ is the bending radius. The large bending radius of NSLS-II, combined with a standard chamber height of 25 mm, results in a cutoff wavelength of 800 μm, effectively removing the portion of the THz spectral range most important for magnetospectroscopy. This provides another compelling reason for a larger dipole chamber and 60 mm gap dipole magnet. Indeed, increasing the dipole gap an additional 30 mm (to accept a 75 mm vertical height chamber) would shift the cutoff wavelength to beyond 4 mm. In all cases, the detailed dipole chamber design and transitions will require careful study in terms of electron beam impedance and potential instabilities. Our initial impedance analysis for a 50 mm high chamber appears promising and suggests that an even larger (75 mm) chamber would be feasible. However, more detailed calculations will be needed for actual chamber mechanical designs to ensure no instability problems will arise.

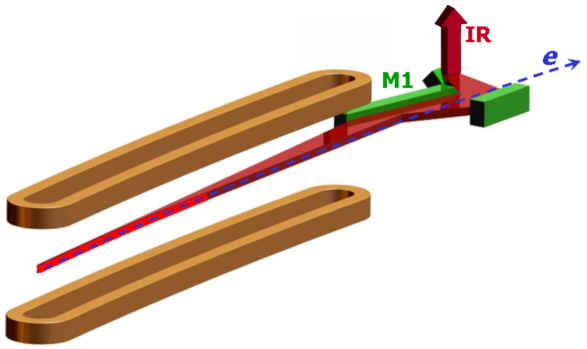

Figure 8.4.2 NSLS-II Infrared Dipole Radiation Extraction. The bright red segment marks the electron beam segment serving as an infrared source. The radiation is collected by a long mirror (M1) and reflected out of the dipole chamber by a second and third mirror combination.

The extraction arrangement for NSLS-II is proposed to have the 1st mirror optic integrated into the dipole chamber construction. The metal mirror can be made to be electrically contiguous with the chamber wall to minimize impedance effects. The oblique angle of incidence and soft x-ray spectrum from the large NSLS-II dipole bending radius limits the local power load on this optic to well under 1 kW/cm^2, such that a special slot or cooling mask may not be required (Figure 8.4.2). Finite element analysis will be performed on candidate mirror materials (e.g., aluminum or copper) to confirm that this heat load can be directly managed without significant optical distortion of the surface. Initial studies of the required optical figure for this 1st mirror suggest that a simple toroidal shape will suffice, allowing conventional diamond turning to be used in its construction (Figure 8.4.3). The remaining optical elements can be either conventional aluminized glass or diamond-turned aluminum to meet specific optical design requirements.

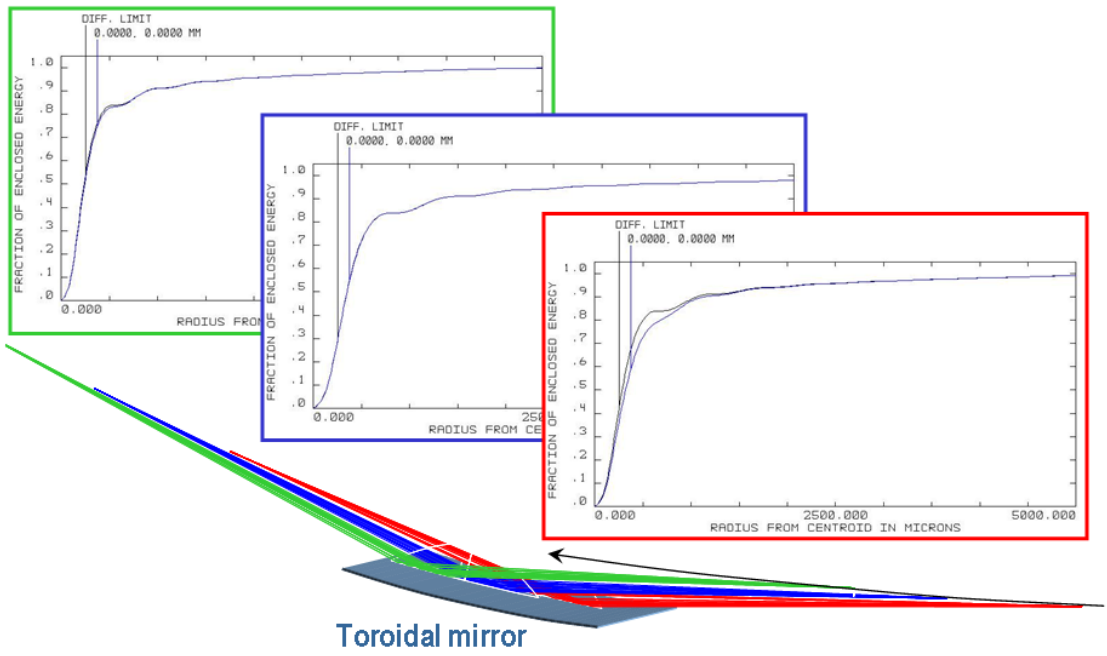

Figure 8.4.3 Extraction Optical Performance. ZEMAX optical analysis for a toroidal first mirror optic when used to focus a dipole bend/arc source at a wavelength of 6 μm (mid-infrared). Near diffraction limited performance is achieved along the entire source length.

A detailed performance comparison for these NSLS-II dipoles and the existing VUV/IR ring dipoles can be made using the standard expressions for dipole synchrotron radiation in the low frequency limit. The flux calculations can be compared to results from other synchrotron radiation source codes such as SPECTRA

[8.4.3] or SRW [8.4.4] to check for consistency. Though some of these calculations are for the photon flux, they can be used for comparing brightness whenever the source's physical dimensions are smaller than the diffraction limit (the case for all IR wavelengths on NSLS-II, and IR wavelengths longer than 10 microns for the existing NSLS VUV/IR ring). We find that all three calculations agree to within 10% for the intrinsic flux of dipole radiation when multiparticle coherence and chamber shielding effects are ignored. Note that one can convert from units of ph/s/0.1%BW to watts per wavenumber, multiplying by 2×10^{-20}. Calculation results are shown in the Figures 8.4.4 and 8.4.5, along with a calculation for an existing port on the VUV/IR ring, indicating that NSLS-II can serve as a highly competitive, and indeed, world-leading, storage ring source for infrared.

Details of these calculation results show that an extraction based on a conventional NSLS-II dipole (average of 16 mrad vertical and 50 mrad horizontal) will be sufficient for mid-infrared spectroscopy, including microprobes and imaging. We envision two options for such mid-infrared extractions. In one option, the beam is divided horizontally to simultaneously serve two or three mid-infrared microprobe end stations. The three collections (in order of entering the dipole) would be (H×V) 15×12 mrad, 15×16 mrad, and 20×20 mrad. The varying vertical aperture is due to the changing distance between the first collecting mirror and the collected source segment as a function of horizontal position (angle). The performance for any of these extractions exceeds the present performance of the NSLS VUV/IR ring over most of the mid-infrared. Only at the long wavelength (low frequency) end of this spectral range are the three extractions distinguishable, with the 20×20 mrad outperforming the other two. But it should be noted that the initial 15×12 mrad collection also includes the zero-degree component, giving this the added feature of edge radiation (not included in the brightness calculation). In the other option, the entire horizontal swath is fed into a single microspectrometer end station based on a focal plane array detector for large area imaging, as described in Chapter 11. The detailed optical system for matching the source to the instrument will be the subject of further research.

In the far-infrared, the brightness for a conventional dipole (16 mrad average vertical extraction) continues to fall away from the ideal value and below the present performance for the NSLS VUV/IR by a factor of 5 at 25 cm^{-1} (400 μm wavelength). The degradation below 10 cm^{-1} becomes even more severe when the shielding effect of the 25 mm high dipole chamber is taken into account. Note that the shielding effect for dipole radiation is a complex subject, and we have taken it into account using a simplified approach. In this approach, it is assumed that radiation unable to couple into a propagating waveguide mode of the chamber is completely lost, and is roughly equivalent to truncating the effective near-field source size to a dimension equal to the chamber height (see [8.4.2], condition 2 for strong shielding). A large-gap dipole enables greater vertical collection efficiency and also shifts the shielding cutoff to lower frequencies. This is illustrated in the brightness calculations of Figure 8.4.5, which includes curves for the standard NSLS-II dipole extraction (50×16 mrad) plus two candidate large-gap dipole extractions (50×32 mrad based on a 50 mm high dipole chamber, and 50×48 mrad based on a 75 mm high dipole chamber). Also shown is the existing performance for the NSLS VUV/IR ring's 90×90 mrad ports plus the very large port beamline at the UVSOR facility (Okazaki, Japan) that represents the most competitive far-infrared beamline elsewhere in the world. (Note: This does not take into account the coherent THz synchrotron radiation mode of operation developed at BESSY and proposed for CIRCE by the ALS/Lawrence Berkeley Lab.) The 50×48 mrad configuration would maintain the NSLS lead in the area of incoherent THz synchrotron radiation, and provide excellent ports for studying aspects of coherent synchrotron radiation production, a subject of great interest for future source development. Any of these ports would offer excellent mid-infrared performance.

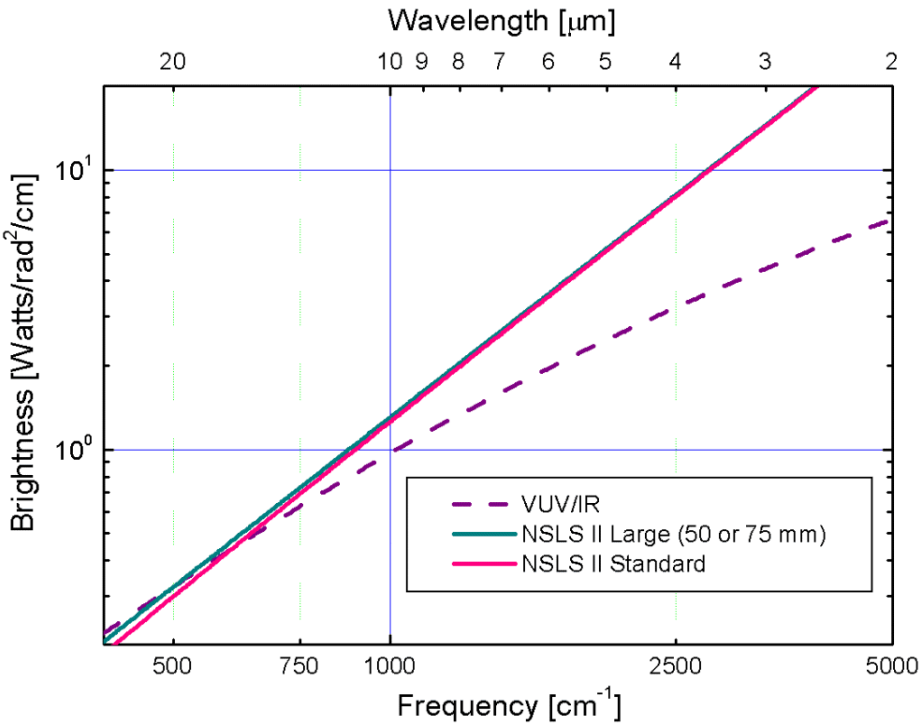

Figure 8.4.4 Calculated NSLS-II brightness for the mid-infrared spectral range, comparing the existing VUV/IR ring with the two proposed for NSLS-II extractions. Note that the lower emittance of NSLS-II leads to brightness improvements over much of this spectral range and that the standard dipole chamber height of 25 mm is sufficient for this spectral range.

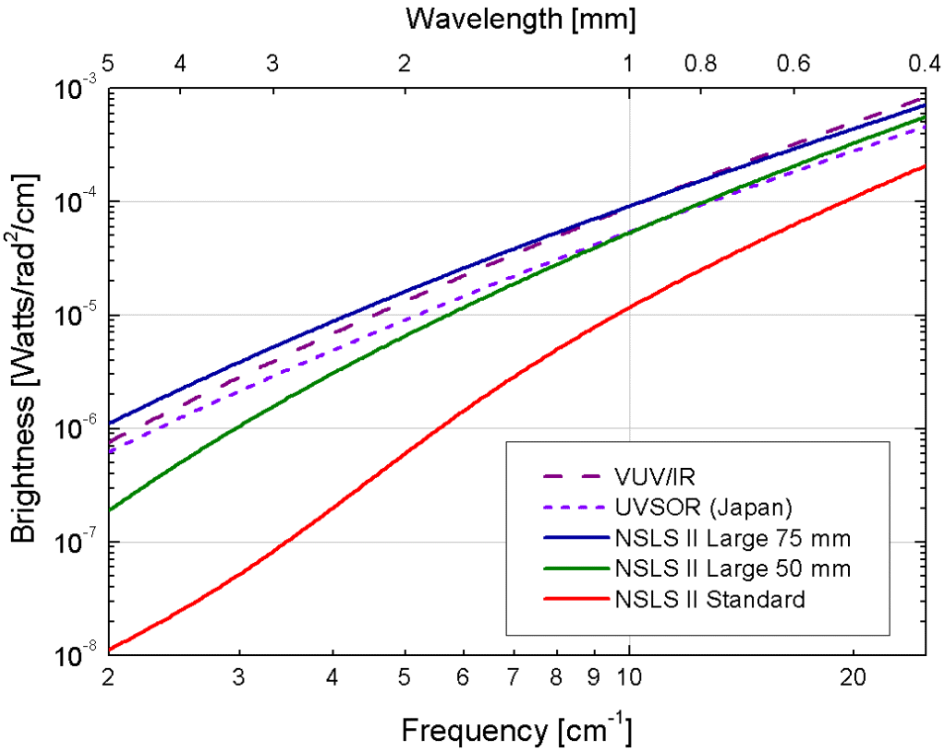

Figure 8.4.5 Calculated NSLS-II brightness for the very far-infrared spectral range, comparing the existing VUV/IR ring with three collection geometries for NSLS-II having vertical dipole chamber heights as shown, plus a high-performance beamline at UVSOR. The cutoff effect of the standard-gap dipole chamber and 16 mrad collection can be clearly seen for wavelengths greater than 1 mm.

8.4.2 Dipole Edge Source

The proposed infrared extraction geometry allows for collection of the zero-degree segment from the dipole (in line with the upstream straight section), including ~5 mrad on the opposite side. This will allow for the extraction of dipole edge radiation [8.4.1]. Dipole edge radiation has characteristics similar to transition or diffraction radiation, e.g., radial polarization. In contrast to bending magnet radiation, the far-field angular distribution for edge radiation is contained mostly within a cone of angle $\theta = 1/\gamma$. This implies an effective source size of $\lambda\gamma$ and a very long formation length of $\lambda\gamma^2$ such that computations designed exclusively for the far-field are no longer accurate. An added complication stems from the fact that dipole edges typically occur in pairs, leading to a ring-like interference pattern that depends on wavelength. The SRW code [8.4.4] includes near-field terms suitable for calculating edge radiation in the ideal case where the ring chamber has no shielding effect on the radiation. An example result from SRW is shown in Figure 8.4.6, and illustrates both edge radiation (ring-like pattern at right) and bend radiation (broad smear extending to left). The actual projection of the beam onto the first mirror optic will be stretched horizontally about a factor of 3 compared to these views (due to the 75° angle of incidence for the radiation).

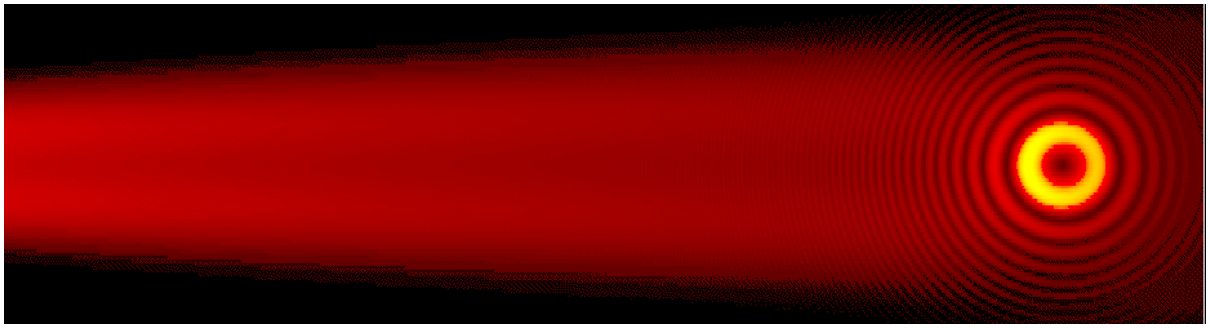

Figure 8.4.6 SRW analysis for 55 mrad (-5 to +50) horizontal and 12 to 20 mrad vertical collection of 6 μm wavelength infrared radiation produced in the leading section of an NSLS-II dipole bending magnet. The ring pattern is due to interference from the back edge of the previous dipole, located 5.6 meters upstream (distance between dipole edges in a DBA cell). The broad stripe of radiation extending to the left is the conventional bending magnet radiation.

Though a few infrared beamlines based on edge radiation exist (e.g., at ANKA/Karlsruhe, SRC/ Wisconsin, and ESRF/Grenoble), the detailed performance at long wavelengths has not been formally demonstrated. There are two reasons to be concerned about the long wavelength performance. First, the radius of the first constructive interference ring moves outward with increasing wavelength such that the collection through a finite aperture will suffer. Second, the large effective source size is expected to cause a shielding (waveguide) cutoff when the wavelength exceeds h^2/R, where h is the chamber height and R is the distance from the source to the collecting aperture [8.4.2]. Our extraction aperture would be situated approximately 3 meters away from the source point and, with a nominal chamber height of 25 mm, the cutoff would begin at a wavelength of ~200 μm such that a significant portion of the very far-infrared would be lost. Edge radiation also introduces complications for mid-infrared microspectroscopy and imaging due to its radial polarization. The source itself is point-like, making it less suitable for illuminating large area focal plane array detectors that are expected to become the standard approach for delivering large area, high-resolution images. For these reasons, our infrared extraction will be based primarily on conventional bending magnet radiation, but we will have the opportunity to exploit the unique characteristics of edge radiation where beneficial.

References

[8.4.1] R.A. Bosch et al., *Rev. Sci. Instr.* **67,** 3346 (1996); Proceedings of the Ninth Nat'l Conf. on Synch. Rad. Instrum., Argonne, IL, (1995.)
[8.4.2] R.A. Bosch, *Nucl. Instrum. & Meth. Phys. Res.* A **482**, 789 (2002).
[8.4.3] T. Tanaka and H. Kitamura, *J. Synch. Rad.* **8**, 1221 (2001)
[8.4.4] O. Chubar and P. Elleaume, *Proc. of the EPAC98 Conference*, 1177 (1998).
[8.4.5] G.L. Carr, *Vibrational Spectroscopy* **19**, 53 (1999); R.P.S.M. Lobo, et al., *Rev. Sci. Instrum.* **73**, 1 (2002).